Adaptation of Extremophilic Proteins with Temperature and Pressure: Evidence from Initiation Factor 6

ARTICLE *in* THE JOURNAL OF PHYSICAL CHEMISTRY B · MAY 2015

Impact Factor: 3.3 · DOI: 10.1021/acs.jpcb.5b02034 · Source: PubMed

7 AUTHORS, INCLUDING:

Paolo Calligari
University of Padova
16 PUBLICATIONS **95** CITATIONS
SEE PROFILE

Vania Calandrini
Forschungszentrum Jülich
30 PUBLICATIONS **242** CITATIONS
SEE PROFILE

Jacques Ollivier
Institut Laue-Langevin
122 PUBLICATIONS **1,017** CITATIONS
SEE PROFILE

Michael Haertlein
Institut Laue-Langevin
138 PUBLICATIONS **2,669** CITATIONS
SEE PROFILE

THE JOURNAL OF PHYSICAL CHEMISTRY B

Article

pubs.acs.org/JPCB

Adaptation of Extremophilic Proteins with Temperature and Pressure: Evidence from Initiation Factor 6

Paolo A. Calligari,*[,†,▽] Vania Calandrini,[‡] Jacques Ollivier,[§] Jean-Baptiste Artero,[§] Michael Härtlein,[§] Mark Johnson,*[,§] and Gerald R. Kneller*[,∥,⊥,#]

[†]SISSA, International School for Advanced Studies, via Bonomea 265, 34136 Trieste, Italy

[‡]Computational Biophysics, German Research School for Simulation Sciences, Jülich, Germany

[§]Institut Laue-Langevin, 6 Rue Jules Horowitz, BP 156, 38042 Grenoble Cedex, France

[∥]Centre de Biophysique Moléculaire, CNRS UPR 4301, Rue Charles Sadron, F-45071 Orléans Cedex 2, France

[⊥]Synchrotron Soleil, L'Orme de Merisiers, BP 48, 91192 Gif-sur-Yvette, France

[#]Université de Orléans, Chateau de la Source-Av. du Parc Floral, 45067 Orléans, France

Supporting Information

ABSTRACT: In this work, we study dynamical properties of an extremophilic protein, Initiation Factor 6 (IF6), produced by the archeabacterium *Methanocaldococcus jannascii*, which thrives close to deep-sea hydrothermal vents where temperatures reach 80 °C and the pressure is up to 750 bar. Molecular dynamics simulations (MD) and quasi-elastic neutron scattering (QENS) measurements give new insights into the dynamical properties of this protein with respect to its eukaryotic and mesophilic homologue. Results obtained by MD are supported by QENS data and are interpreted within the framework of a fractional Brownian dynamics model for the characterization of protein relaxation dynamics. IF6 from *M. jannaschii* at high temperature and pressure shares similar flexibility with its eukaryotic homologue from *S. cerevisieae* under ambient conditions. This work shows for the first time, to our knowledge, that the very common pattern of *corresponding states* for thermophilic protein adaptation can be extended to thermobarophilic proteins. A detailed analysis of dynamic properties and of local structural fluctuations reveals a complex pattern for "corresponding" structural flexibilities. In particular, in the case of IF6, the latter seems to be strongly related to the entropic contribution given by an additional, C-terminal, 20 amino-acid tail which is evolutionary conserved in all mesophilic IF6s.

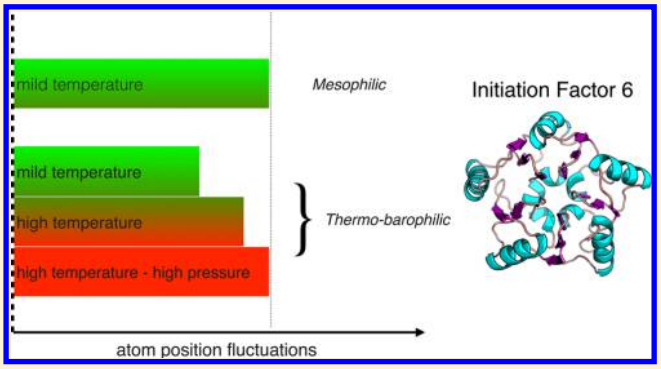

INTRODUCTION

The adaptation of living organisms to extreme environmental conditions is one of the most challenging areas in molecular biology.[1] In the last decades, particular interest has been devoted to organisms which live in the deep sea near hydrothermal chimneys, where the temperature can change over small distances from 4 °C up to 100 °C and pressure may reach values of around 800 bar.[2] In this kind of environment, the conditions of chemical equilibrium in biological systems are altered. In most cases, organisms find a way to adapt to these conditions using a global optimization of molecular structures and metabolic pathways.[3] The central issue in adaptation is the conservation of biological functionality which requires a subtle balance between stability and flexibility.[4−6]

Evolution therefore modifies the physicochemical properties of thermophilic proteins to match the molecular properties of mesophilic counterparts.[7] Translation to a different environment is performed by a reorganization of noncovalent interactions which creates *corresponding states* in topologies and structural flexibility between homologous proteins at their respective *in situ* conditions. The corresponding states principle, schematically sketched in Figure 1, was first formulated by Vihinen[8] and Jaenicke.[7] In the context of thermophilic proteins, evidence for such processes was provided both by experiments[9−11] and by molecular dynamics (MD) studies.[12] However, while this idea has found several confirmations in the past, some recent works are ambiguous in this respect.[13,14]

Quasi-elastic neutron scattering (QENS) experiments are particularly suited to explore protein dynamics on an atomic level within the nanosecond time scale.[15−22] They need to be performed in dilute solution to avoid protein agregation, which means that the signal-to-noise ratio is low. In addition, pressure cells increase the background further. In this situation, MD simulations can be combined with QENS which allows the

Received: March 2, 2015
Revised: May 7, 2015
Published: May 21, 2015

DOI: 10.1021/acs.jpcb.5b02034
J. Phys. Chem. B 2015, 119, 7860−7873

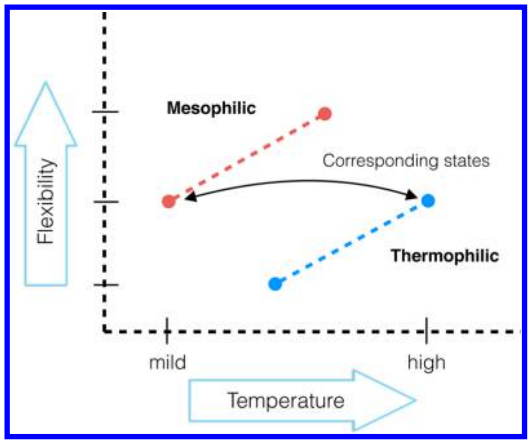

Figure 1. Schematic representation of the well-known *corresponding states* principle for thermophilic adaptation: mesophilic and thermophilic proteins share the same flexibility at mild and high temperatures, respectively. According to the same principle, thermophilic proteins show lower flexibility than their mesophilic counterparts at ambient temperature.

numerical models to be validated and the experimental data to be fully exploited.

In this work, we have used such a combined approach to explore the effects of *deep-sea* pressure (lower than 1 kbar) and high temperatures on the dynamics of a protein produced by the archaeon *Methanocaldococcus jannaschii*, which thrives at more than 2600 m below sea level and at temperatures of around 80 °C. Adaptation to high pressure environments is usually considered as a secondary adaptation process which may not be completely fulfilled by molecular evolution.[23] The effective role of pressure in determining the native structural state and dynamical properties of extremophilic proteins therefore needs to be thoroughly investigated. Proteins from *M. jannaschii* are counterparts of choice in comparison with homologous proteins from eukaryotic organisms,[10,24−26] but their hyperthermophilic origin (produced by organisms living at very high temperature) has been investigated much more intensively than their possible barophilic character (i.e., the fact that the organism thrives under relatively high pressures).[27,28] Considering both of these aspects should reveal more complex behavior as demonstrated in other cases.[12,29] We have studied the dynamics of the protein Initiation Factor 6 (IF6) from *M. jannaschii*[30] (aIF6) in comparison with its homologue from eukaryotic *Saccharomyces cerevisiae* (eIF6). IF6s are an appropriate target for our study, since they are involved in ribosome biosynthesis and limit the rate of translation of RNA in ribosome.[31,32] Moreover, their optimal activity is crucial for cell global fitness[33−35] and they are particularly sensitive to external stimuli and to the global status of the cell.[30,33,36]

The influence of pressure and temperature on the dynamics of the two IF6 is interpreted with an analytical model for QENS spectra which accounts for the multiscale relaxation dynamics in complex systems like proteins.[37] In this model, the atomic motions are described by a fractional Ornstein−Uhlenbeck (fOU) process,[38,39] a non-Markovian extension of the well-known normal Ornstein−Uhlenbeck process,[40] which describes anomalous diffusion of a Brownian particle in a harmonic potential. Fractional Brownian dynamics models in general were shown to be highly effective in describing environmental effects on protein dynamics over a large range of time scales (from sub-nanoseconds to hours).[41−50]

RESULTS

Sequence and Structure Analysis of aIF6 and eIF6.

A detailed comparison of IF6 structures was given by Groft and co-workers.[30] Here, we recall the main properties that will be useful in the following discussion. In terms of the primary sequences, the two IF6s (Table 1) show a rather typical picture in the extremophilic/mesophilic comparison:[51,52] aIF6 has more charged residues and less polar hydrophilic residues than eIF6.

Table 1. Comparison of the Percentage of Groups of Amino Acid Residues[a]

structure	DEKR	ACFILMPVWY	HNQST	G
aIF6	24.5	45.5	21.0	8.8
eIF6	18.8	43.9	29.0	8.2
aIF6-htag	23.0	43.5	24.2	9.3
eIF6-not	17.9	45.0	28.6	8.5

[a]Groups of amino acids (represented by their one-letter codes) include charged (DEKR), hydrophobic (ACFILMPVWY), and hydrophilic (HNQST). Glycine (G) is kept separate.

The two IF6 homologues share a highly conserved structure made of five almost-symmetric structural subdomains with ∼30% identical sequences. aIF6 has a slightly longer α-helix (residues 78−90), while eIF6 has an additional highly disordered C-terminal tail of ∼20 amino acids (Ctail).

Both IF6s show an unusual structural pattern in their evolutionary conserved structure (see Figure 2): hydrophobic cores of the five subdomains form a "hydrophobic torus" instead of a single global central core.[30] This toroidal pattern is created by side chains of the buried β-strands and creates in turn a *cave-like* hollow in the center of the overall structure. The opening of this central hollow has a diameter of ∼7 Å, and the presence of water molecules in crystallographic structures suggests that water may flow through it in solution.

A BLAST analysis of the additional Ctail fragment against the UniProtKB/SwissProt sequence database gave significant scores only from eukaryotic IF6 homologues (see the Supporting Information), thus suggesting a specific role for this protein family. This idea is comforted by recent works which show the contribution of the C-terminal subdomain to the localization of eIF6 in the cellular nucleus.[32,53] Moreover, although truncation of Ctail in eIF6 seems to have slight effects in antiassociation functionality,[30] information is lacking for all other functions performed by eIF6 in eukaryotic cells.

A highly unstructured and mobile Ctail was suggested by the absence of experimental information from X-ray crystallography.[30] Nonetheless, its secondary structure is predicted to be not completely unstructured by two distinct methods (PSIPRED server[54] and APSSP2 server[55]). Both methods predict an α-helix at the end of the fragment, in the region Asp238-Glu241. These results are consistent with the hydrophobic profile of the fragment (Kyle/Doolittle scale[56]) which shows an increasing hydrophobicity in the regions Pro229-Ser231 and Asp238-Glu242. We confirmed the presence of a partially folded structure by a set of preliminary MD simulations of a freely moving Ctail and with a harmonic restraint for N-terminal C_α positions. In both simulations, the predicted α-helix was folded within a few tens of nanoseconds (see the Supporting Information). Overall, these findings indicated the importance of maintaining the 21 C-terminal

DOI: 10.1021/acs.jpcb.5b02034
J. Phys. Chem. B 2015, 119, 7860−7873

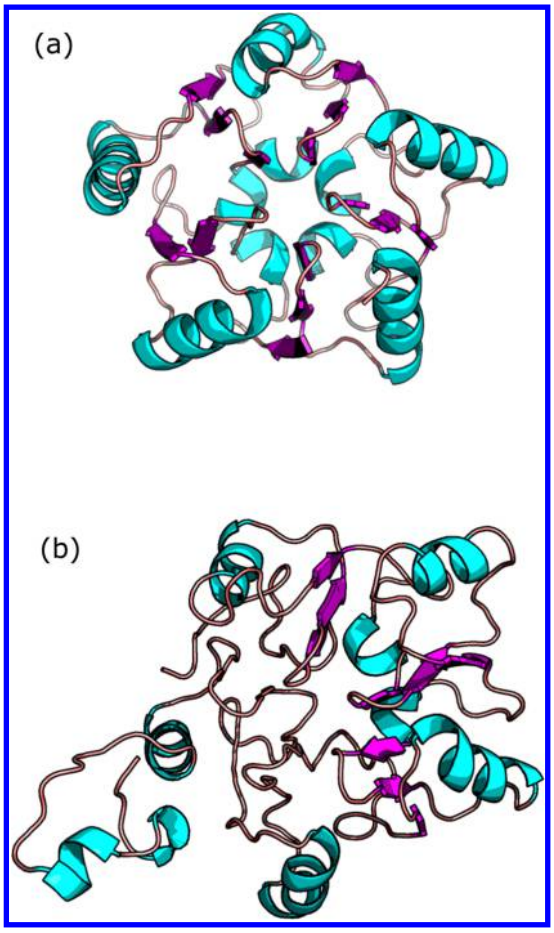

Figure 2. Three-dimensional structures of aIF6 (panel a, PDB code: 1G61[30]) and eIF6 (panel b, see Supporting Information). The coloring scheme highlights the secondary structure motifs of each structure.

fragment as part of the investigated protein for it could have a significant role in the dynamics and structure stability of eIF6.

In this context, it is interesting to note that, despite their rather similar structure, aIF6 is able to reversibly respond to high temperature values,[30] while eIF6 is known to undergo inactivation at 330 K.[57] To verify the stability of the samples used in this work, we performed dynamic light scattering measurements on eIF6 (Table 2). The results are in very good agreement with previous works and show that eIF6 may undergo a partial unfolding or aggregation already at 320 K, with the hydrodynamic radius increasing from 3 nm to almost 30 nm. Moreover, when brought back to 300 K, the original hydrodynamic radius is not recovered, suggesting that the transition is not reversible. Neutron scattering measurements on eIF6 were therefore limited to ambient conditions. MD simulations were however performed on eIF6 at high temperature and high pressure as a reference for further discussion.

Table 2. Variation of the Hydrodynamic Radius of Eukaryotic eIF6[a]

	290 K	300 K	320 K	back to 300 K
R_H (nm)	3.32	3.61	29.76	24.23

[a]Reported values of hydrodynamic radius at 290 K correspond to a spherical approximation of the whole protein structure.

QENS Spectra and Internal Dynamics. In Figure 3, we report the measured and calculated incoherent dynamic structure factors (IDSFs) of aIF6 and eIF6. Table 3 summarizes all the thermodynamic conditions studied in this work, experimentally or computationally.

IDSFs from MD were compared to the experimental ones using eq 10 where the apparent global translation diffusion coefficient in $S_g(.)$ was set as a free parameter (see red curves in Figure 3). As a consequence of the hollow central opening, the IF6 hydrodynamic overall shape is better approximated by a torus rather than a sphere. This observation is confirmed by the obtained diffusion coefficients $D_a^{300} = 51.8 \times 10^{-3}$ Å^2/ps and $D_a^{350} = 92.66 \times 10^{-3}$ Å^2/ps for aIF6, which are very close to the theoretical values for translation diffusion of toroidal structures calculated from the average MD structures (see eq 12 in the Materials and Methods section): $D_{torus}^{300} = 42.84 \times 10^{-3}$ Å^2/ps and $D_{torus}^{350} = 95.36 \times 10^{-3}$ Å^2/ps.

The QENS spectra in Figure 3 show good agreement with MD spectra on the sub-nanosecond time scale given the above fitting scheme. The high-pressure measurements on aIF6 were performed on a polyhistidine-tagged protein in order to improve the yield of sample purification and enhance the signal-to-noise ratio. Measurements on this kind of sample may still be affected by artifacts,[58] and MD simulations of polyhistidine-tagged aIF6s (aIF6-htag) were used for comparison with the experimental results. Both techniques therefore show significant effects of temperature (panel a vs panel b and panel c vs panel d) and pressure (panel a vs panel c and panel b vs panel d) on aIF6.

Mean-Square Displacement. Temperature and pressure induced trends are seen clearly in the time-dependent mean-square displacement (MSD) computed from MD trajectories (Figure 4). MSDs show pronounced increases with increasing temperature. They reveal that eIF6 at 300 K as well as aIF6 at 350 K are relatively insensitive to pressure; there is a small decrease in the MSD, whereas they undergo a more evident change at their respective *non-natural* temperatures. At high temperature, eIF6 also shows a large change due to pressure when compared to room temperature data, which is reminiscent of the preliminary steps of a nascent unfolding process eIF6 that is not accessible on the sub-nanosecond time scale (see Table 2).

IDSFs and MSDs show that aIF6-htag (panel c, Figure 4) undergoes effects similar to eIF6, suggesting that it may share some dynamical properties with the latter rather than with aIF6. The outcome of this finding will be discussed in more detail in the following sections.

Spectra from both eIF6 and aIF6-htag are due to the convolution of different contributions to the global signal: the overall protein motion (translation and rotation), internal dynamics of the toroidal conserved structure, and diffusive dynamics of N- or C-terminal tails in water. In this context, MD simulations help to separate these contributions and focus only on the internal dynamics of the evolutionary conserved toroidal domain, thus allowing a direct comparison between the two homologues. For this reason, all of the quantities of interest presented in the following were calculated only for the evolutionary conserved region 1−224 of each IF6. While this approach excludes the direct contribution of the motion of terminal parts of eIF6 and aIF6-htag, it is important to

DOI: 10.1021/acs.jpcb.5b02034
J. Phys. Chem. B 2015, 119, 7860−7873

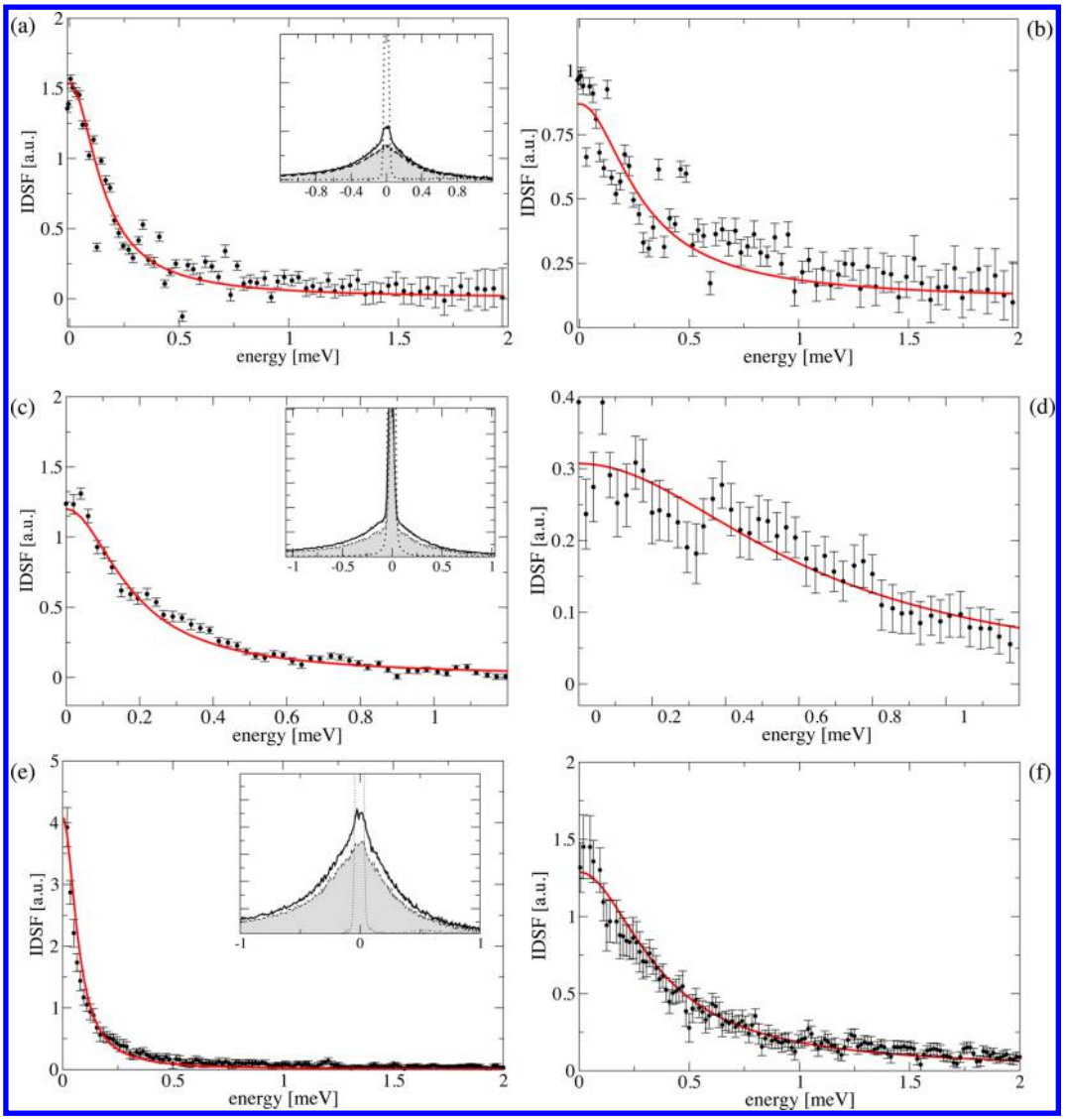

Figure 3. Incoherent dynamic structure factors (IDSFs) for aIF6, eIF6, and aIF6-htag at different temperatures and pressures. Experimental QENS spectra (points with error bars) are compared with and dynamic structure factors obtained by MD simulations and convoluted with fitted translational diffusion (red lines). Data for aIF6 at 300 K and 1 bar (panel a) and 350 K and 1 bar (panel b) are shown for q = 18 nm^{-1}. High-pressure experimental data from aIF6-htag shown in panel c (300 K, 500 bar) and panel d (350 K, 500 bar) are for q = 17.2 nm^{-1}. Panels e and f show spectra from eIF6 at 300 K for q = 5.7 nm^{-1} and q = 18 nm^{-1}, respectively. Raw spectra from protein solutions (black line), solvent (gray shaded lines), and vanadium (dotted lines) are presented in the insets of panels a, c, and e to show the different contributions to the measured spectra.

Table 3. Samples Studied in This Work[a]

		aIF6	eIF6	aIF6-htag	eIF6-not
300 K	1 bar	FOCUS, MD_2	FOCUS, MD_2, MD_{50}	MD_2	MD_2
	500 bar	MD_2	MD_2	IN6, MD_2	MD_2
350 K	1 bar	FOCUS, MD_2, MD_{50}	MD_2	MD_2	MD_2
	500 bar	MD_2	MD_2	IN6, MD_2	MD_2
	750 bar	MD_2, MD_{50}			
	1 kbar	MD_2			

[a]Different methods were used: QENS data were obtained from FOCUS (PSI, Zurich) and IN6 (ILL, Grenoble) spectrometers; MD simulations were performed to obtain 2 and 50 ns long molecular dynamics trajectories (MD_2 and MD_{50}, respectively). aIF6-htag and eIF6-not stand for the polyhistidine-tagged aIF6 C-terminal-cleaved eIF6, respectively.

note that these dynamics affect the motions of the rest of the protein.

Fractional Brownian Dynamics Model. Internal dynamics of the two IF6s can be investigated by the analysis of time correlation functions, intermediate scattering functions (ISFs), which can be directly computed from the MD trajectories (Figure 5). The ISFs show the same trends as the MSDs, albeit with a Q-dependence. ISFs decay markedly with increasing

DOI: 10.1021/acs.jpcb.5b02034
J. Phys. Chem. B 2015, 119, 7860−7873

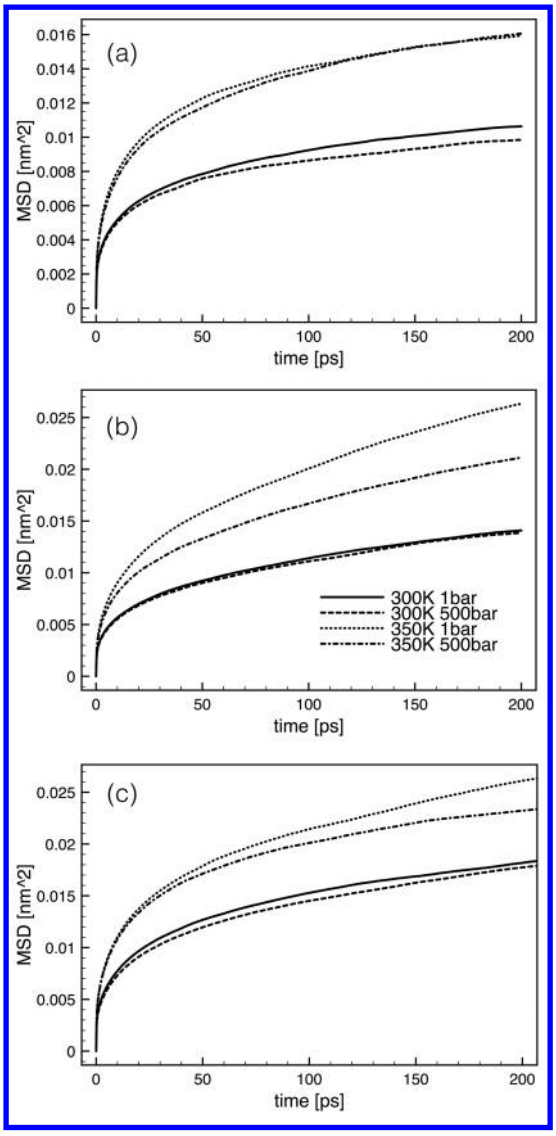

Figure 4. Time-dependent atomic mean-square displacement (MSD) at different temperatures and pressures for aIF6 (panel a), eIF6 (panel b), and aIF6-htag (panel c). The same line style is used in all figures, and it is referred to in panel b.

temperature, due to larger amplitude motions, while the pressure-induced changes, corresponding to reduced amplitude motions, are smaller, except for eIF6 at 350 K which is due to unfolding.

The ISFs are analyzed with a model for QENS spectra, where atomic motions are described by a fractional Ornstein–Uhlenbeck (fOU) process.[37] The well-known "normal" Ornstein–Uhlenbeck process describes the diffusion of a Brownian particle in a harmonic potential,[40] and the resulting position autocorrelation function decays exponentially. The fractional counterpart owes its name to a fractional time derivative which appears in the Fokker–Planck equation for the transition probability[38,39] and which can be considered as a mathematical trick to make the resulting position correlation function decay with a power law. The latter behavior can be expressed by a continuous spectrum of relaxation rates[37] which reflects the self-similar multiscale relaxation dynamics of proteins.[41−48] Assuming the atomic motion to be isotropic and that the internal dynamics of the predominantly incoherently scattering hydrogen atoms can be described by one "representative" atom, the intermediate scattering function corresponding to an fOU process may be written as[37]

$$I(q, t) = \exp(-q^2\langle x^2\rangle) \sum_{n=0}^{\infty} \frac{q^{2n}\langle x^2\rangle^n}{n!} E_\alpha(-[t/\tau_n]^\alpha) \quad (1)$$

where $\tau_n = \tau n^{-1/\alpha}$ and τ sets the time scale. With $\langle x^2\rangle$, we denote the ensemble averaged square atom position fluctuation of the representative atom and $E_\alpha(z)$ is the Mittag–Leffler function[59]

$$E_\alpha(z) = \sum_{k=0}^{\infty} \frac{z^k}{\Gamma(1 + \alpha k)} \quad (2)$$

Here $\Gamma(z)$ is the Gamma function (generalized factorial) and the Mittag–Leffler function is an entire function, which is defined everywhere in the complex plane. For $\alpha = 1$, it reduces to the exponential function. The intermediate scattering function (eq 1) is thus a superposition of "stretched" Mittag–Leffler functions. Each of these functions may be expressed as

$$E_\alpha(-[t/\tau]^\alpha) = \int_0^\infty d\lambda\, p(\lambda; \alpha) \exp(-\lambda[t/\tau]) \quad (3)$$

where $p(\lambda; \alpha)$ is a dimensionless relaxation rate spectrum whose form is determined by the parameter α

$$p(\lambda; \alpha) = \frac{\sin(\pi\alpha)}{\pi\lambda(\lambda^{-\alpha} + \lambda^{\alpha} + 2\cos(\pi\alpha))} \quad (4)$$

In the limit $\alpha \to 1$, the relaxation rate spectrum becomes $p(\lambda; \alpha) = \delta(\lambda - 1)$, indicating "pure" exponential relaxation, and correspondingly $E_\alpha(-[t/\tau]^\alpha) \to \exp(-t/\tau)$. In the range $0 < \alpha < 1$, the function 3 exhibits a power-law decay for $t \gg \tau$, $E_\alpha(-[t/\tau]^\alpha) \sim (t/\tau)^{-\alpha}/\Gamma(1 - \alpha)$.

The insets of Figure 5 display the fits of the model (eq 1) to the simulated intermediate scattering function of aIF6 and eIF6, and the corresponding fit parameters for different values of momentum transfer and various environmental conditions are presented in Figure 6. The fact that the α-parameter is clearly below 1 indicates a strongly nonexponential decay of each term in the sum (eq 1). It should be noted that, in the framework given by eq 1, $\langle x^2\rangle$ is a Q-dependent quantity (in contrast to the Q-independent MSD) which is obtained directly from eq 9. It represents, in fact, an *apparent* mean square position fluctuation which is seen by the neutrons at different Q-values. aIF6 and eIF6 show two significantly different properties: τ in eIF6 is generally larger than that in aIF6 by a factor of 4, meaning that the internal dynamics are characterized by significantly slower motions; α values for aIF6, although similar, indicating similar effective potentials, are systematically slightly larger than those for eIF6.

As expected, both α and τ decrease with temperature at all pressure conditions. Accordingly, $\langle x^2\rangle$ increases with temperature, while it is slightly reduced by pressure. In particular, aIF6 seems to be systematically more rigidly packed than eIF6 under all conditions. Of note, the two IF6 have relatively similar $\langle x^2\rangle$ at their respective *natural* conditions (i.e., the physiological thermodynamic conditions for the hosting organism). Moreover, aIF6 and eIF6 show comparable values of α but significantly different values of τ in all combinations of temperature and pressure.

DOI: 10.1021/acs.jpcb.5b02034
J. Phys. Chem. B 2015, 119, 7860−7873

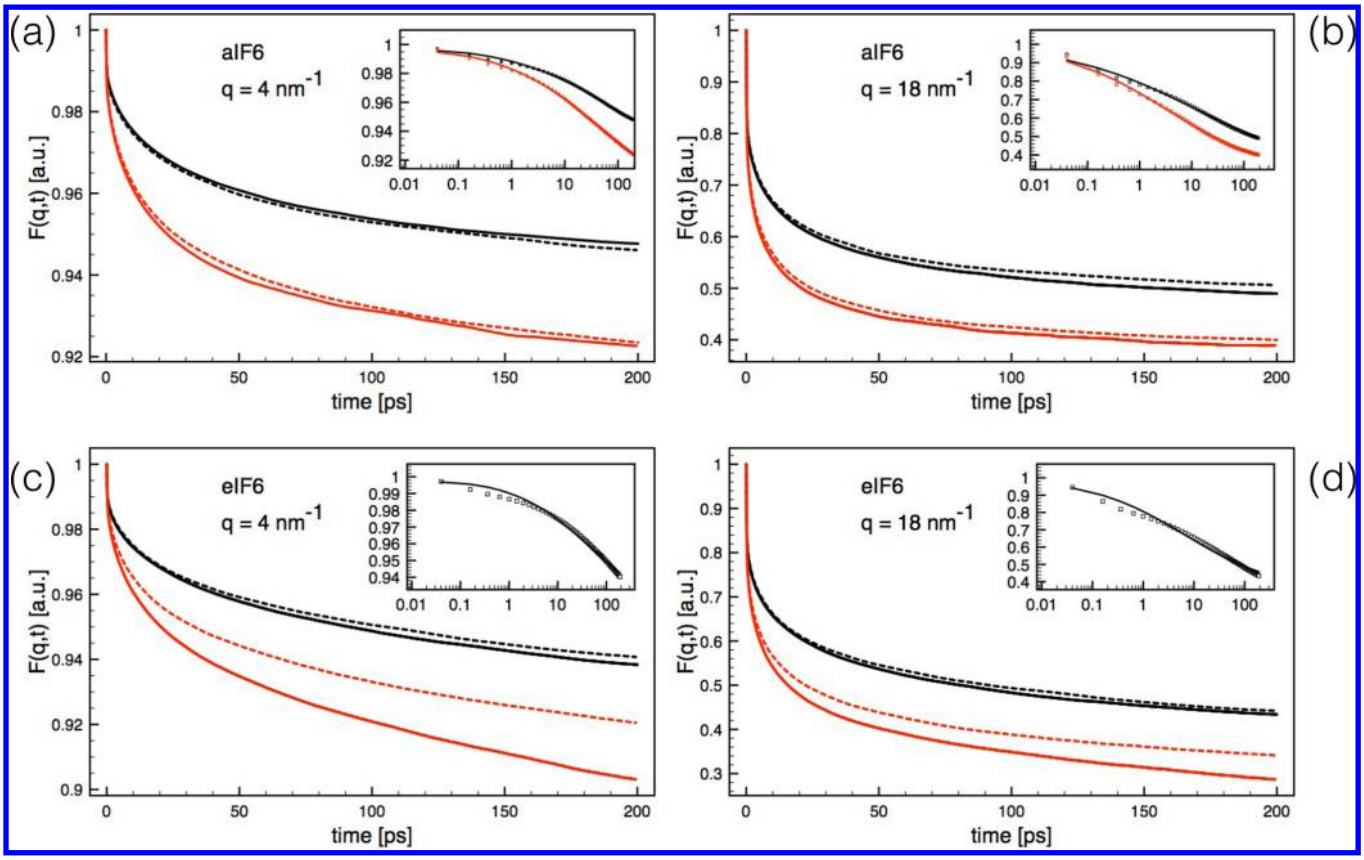

Figure 5. Intermediate scattering function (ISF) of aIF6 (panels a and b) and eIF6 (panels c and d) calculated from MD simulations at different combinations of temperature and pressure. ISF from data at 300 and 350 K (black and red lines, respectively) and 1 and 500 bar (solid and dashed lines) are shown for two different q-values (4 and 18 nm^{-1}). Insets in each figure show the calculated ISF compared with the fOU model for three representative cases: aIF6 at 300 K and 1 bar and 350 K and 500 bar (black and red data, respectively) and eIF6 at 300 K and 1 bar.

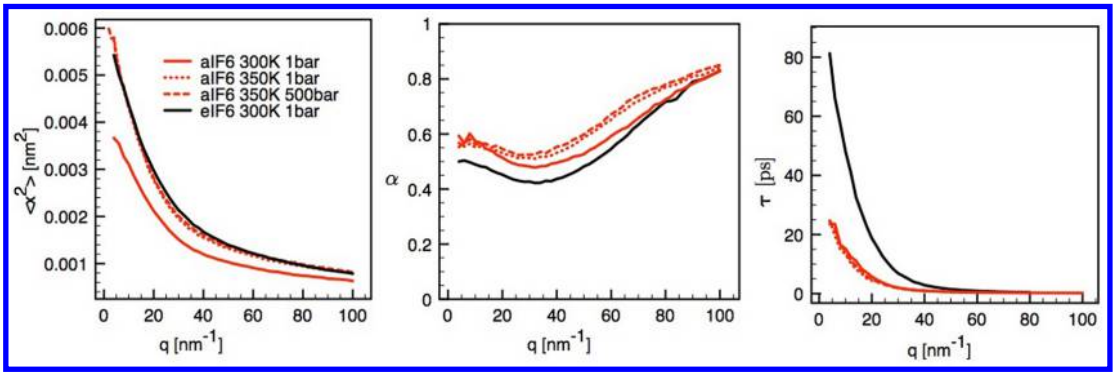

Figure 6. Parameters obtained from the comparison of ISF computed from MD simulations and eq 1. The value of $\langle x^2 \rangle$ is given according to eq 9 and was kept fixed on fits.

These findings are reminiscent of the *corresponding states* hypothesis, which states that thermophilic proteins show an enhanced conformational rigidity in the folded native state at room temperature and reach the flexibility of their mesophilic homologues at higher temperatures. Similar results have been obtained by Tehei and co-workers[11,25] from the comparison of MD simulations in other thermophilic and mesophilic proteins. These results suggest that this hypothesis is also applicable for thermo-barophilic proteins when both temperature and pressure are taken into account.

Elastic Incoherent Structure Factor. Further analysis of the rigidity/flexibility of IF6 focuses on the analysis of the elastic incoherent structure factor (EISF), which is related to the configurational space volume explored by atomic motions in macromolecules and is widely used to characterize conformational variability of proteins.[60,61] EISFs confirm that aIF6 is clearly more rigid than eIF6 at room temperature (Figure 7), while the two IF6 become, again, very similar to each other when compared at their respective physiological temperatures. This correspondence of EISFs is "fine-tuned" when pressure is applied. Differences between EISFs from aIF6 at different conditions and EISFs from eIF6 at ambient conditions help to clarify this point (Figure 8). aIF6 is slightly more rigid than eIF6 in the q-range 15−40 nm^{-1} with a maximum at $q \sim 25$ nm^{-1}. Interestingly, this range in the reciprocal space corresponds to 1.5−4 Å in real space, i.e., to the local

DOI: 10.1021/acs.jpcb.5b02034
J. Phys. Chem. B 2015, 119, 7860−7873

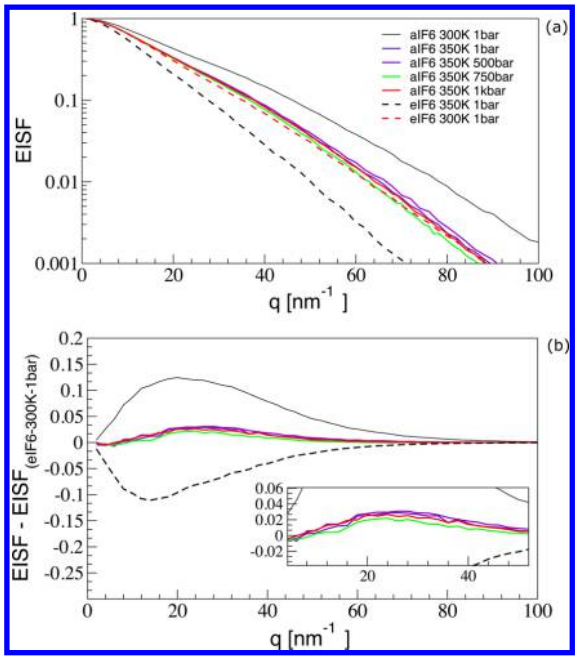

Figure 7. Panel a: Comparison of EISFs at different temperatures and pressures for aIF6 and eIF6, calculated from MD simulations. Panel b: Differences between EISFs for aIF6 at different thermodynamic conditions and EISFs from eIF6 at 300 K and 1 bar. The color scheme is the same in both figures. The inset shows a zoom on the main figure, highlighting the similarity of the EISFs in the central bundle.

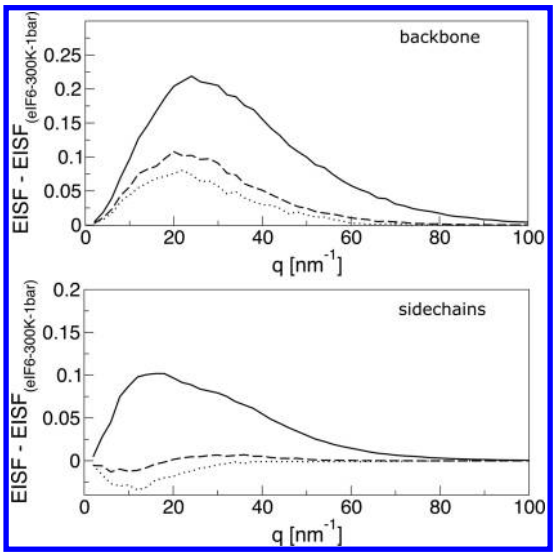

Figure 8. Differences of EISFs from a selected group of atoms (upper panel, backbone atoms; lower panel, side chain atoms) between aIF6 at 300 K and 1 bar (solid line), 350 K and 1 bar (dashed line), 350 K and 750 bar (pointed line) and eIF6 at 300 K and 1 bar.

fluctuations of amino acids. Moreover, this small difference does not significantly increase with pressures higher than 750 bar, which corresponds to the optimal pressure for growth and methanogenesis of *M. jannaschii*.[28] We note in this context that Figures 7 and 8 compare EISFs of two variants of the same protein, which have essentially the same normal mode spaces. Differences in the EISFs reflect thus different motional amplitudes for the same normal modes, and thus different rigidity.

A more detailed picture of the dynamical effects induced by extreme conditions may be given by calculating the EISF selectively for backbone and side chain atoms, as shown in Figure 8. Here, a direct comparison of differences between EISFs at "natural" conditions of the two homologues shows that aIF6 have a 6% more rigid backbone than eIF6 (positive difference). Conversely, side chains show an opposite tendency with aIF6 about 2% more flexible than eIF6 (negative difference). Additionally, this analysis also suggests that pressure has a role in "fine-tuning" the right stiffness over the whole q-range for both backbone and side chain atoms. In particular, pressure at high temperature seems to loosen aIF6 instead of rigidifying it, as it is at ambient temperature.These variations do not correspond to changes in molecular shape as probed by solvent accessible surface area (SASA). For aIF6 and eIF6, SASAs are rather similar, being 104.25 and 103.1 Å^2, respectively, and significant variations are induced only by temperature, albeit to a limited extent (ΔSASA = 1.1 Å^2 for aIF6 and ΔSASA = 3.2 Å^2 for eIF6). These findings suggest that changes in atomic fluctuations related to EISFs at different environmental conditions are not correlated with an overall change in the surface exposed to the solvent.

Local Flexibility. Results presented and discussed so far arise from fast rotational and vibrational motions of amino acids (mostly from motions of their side chains, along the C−C bonds) which are observable by QENS-validated EISFs on the sub-nanosecond time scale. To further investigate the heterogeneity in atomic fluctuations, we have calculated the atomic root-mean-square position fluctuations, RMSF(i) = $(\langle \mathbf{R}_i - \langle \mathbf{R}_i \rangle \rangle^2)^{1/2}$, from two sets of MD trajectories giving access to different time scales.

The average RMSFs obtained from these simulations (Table 4) show that aIF6 is slightly more rigid than eIF6 at ambient temperature both on the picosecond and nanosecond time scales. Similar results have been found in other comparisons between thermophilic and mesophilic proteins.[62] However, in agreement with observations from MSDs and EISFs (above), the C_α-RMSFs from aIF6 at high-temperature/high-pressure conditions are closer to the ones of eIF6 at ambient conditions than for any other aIF6 under "non-optimal" conditions (see Figure 9). A more complex picture comes to light when RMSFs are compared with local structural motifs.

Overall, eIF6 shows generally larger fluctuations than aIF6 in loop regions. The RMSF of eIF6 has also a slightly higher *baseline*, which is particularly evident for residues from 160 to 225. This difference between RMSFs is essentially due to the presence of the Ctail in eIF6 which transmits additional fluctuations to the rest of the protein. Large changes with respect to temperature and pressure are found for aIF6 in unstructured regions between helices and β-strands. Concerning backbone position fluctuations, temperature has a leading effect, while pressure induces changes in RMSFs smaller than 0.5 Å (see lower panel of Figure 10). These results are compatible with the corresponding states hypothesis albeit limited to the sub-nanosecond time scale.

Further insight can be gathered from the analysis of the longer MD$_{50}$ simulations. We note here that removing global motions of eIF6 on this time scale becomes difficult, as the effects of Ctail diffusion on the overall protein motion are not negligible and internal motions cannot be easily isolated. To overcome this difficulty and allow for a direct comparison between eIF6 and aIF6, the fluctuations of local variables which are not affected by overall protein motion can be studied.

DOI: 10.1021/acs.jpcb.5b02034
J. Phys. Chem. B 2015, 119, 7860−7873

Table 4. Average All-Atom Root Mean Square Fluctuations[a]

⟨RMSF⟩ (Å)		eIF6	aIF6	aIF6-htag	eIF6-not
300k	1 bar	1.05 (*1.22*)	0.80 (1.11)	0.96	0.86
350k	1 bar	1.54	0.99 (1.26)		
	500 bar	1.20	1.01 (1.23)	1.17	1.00
	750 bar		(1.19)		

[a]Values in brackets are from MD_{50}. eIF6 RMSF from MD_{50} are calculated after removing global motions by aligning only residues 1−224: its value may be affected by spurious contributions of Ctail motions to internal motions of aligned residues and should be taken only as a qualitative reference.

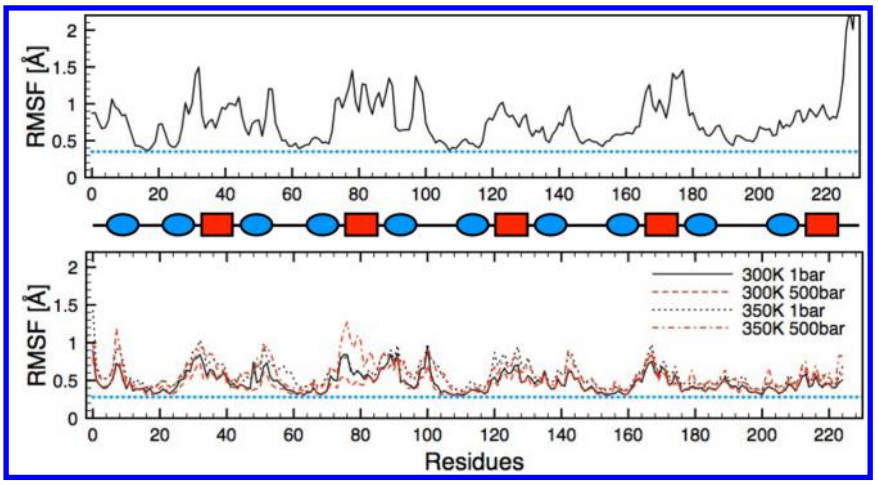

Figure 9. RMSF of carbon C_α in eIF6 (upper panel) and aIF6 (lower panel). A schematic representation of the secondary structure profile of IF6 is shown at the middle of this figure. Rectangles and ellipses represent α-helices and β-strands, respectively.

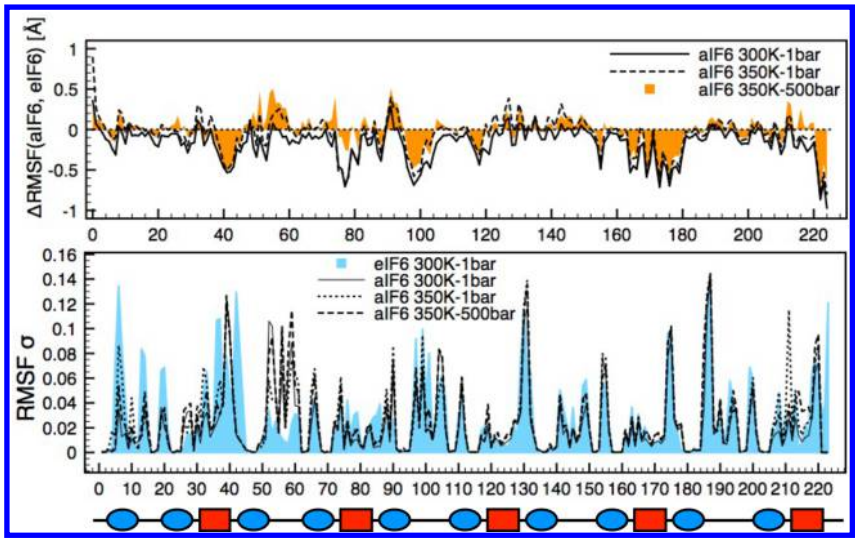

Figure 10. Upper panel: Differences of carbon C_α RMSF between aIF6 at different conditions and eIF6 at 300 K and 1 bar. Lower panel: Mean square fluctuations of the *straightness* σ parameter which is the scalar product of locally defined axes of rotation for the backbone. σ is a measure of local backbone flexibility (see the Materials and Methods section for details).

The mean square fluctuations of the straightness parameter σ (see the Materials and Methods section) gives a measure of the backbone local bending, i.e., flexibility during MD simulations. Here, the analysis of $\langle \Delta\sigma^2 \rangle$ shows very few regions where eIF6 and aIF6 are notably different (see Figure 10). Changes occur in regions which are mostly located in the N-terminal domain, and they correspond to regions where changes in RMSF were found in MD_2.

These results suggest that IF backbones are only slightly affected by high pressure and high temperature on the nanosecond time scale. Conversely, extreme conditions have a significant impact on overall side-chain mobility. This point is illustrated by Figure 11 which shows the distribution of side-chain dihedral angle order parameters Θ_χ (see the Materials and Methods section) for each IF. The quantity Θ_χ gives a quantitative estimation of the fluctuations of each side chain along a MD simulation.[63] Therefore, the distribution of all Θ_χ in a protein gives a measure of the overall flexibility of protein side chains. Due to their significantly asymmetric shape, the distributions obtained here are more appropriately compared

DOI: 10.1021/acs.jpcb.5b02034
J. Phys. Chem. B 2015, 119, 7860−7873

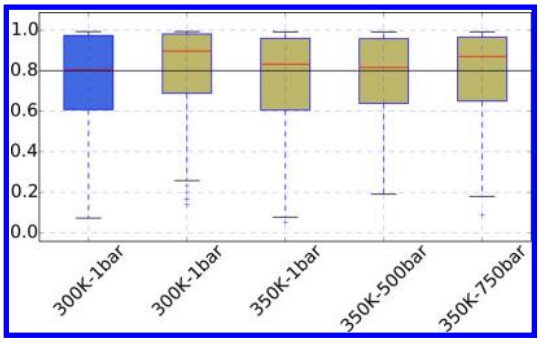

Figure 11. Global mobility of eIF6 (blue) and aIF6 (green) by side-chain dihedral angle order parameters defined by eq 13 and calculated from MD_{50}. The red horizontal line inside each box indicates the median values; box edges indicate the upper and lower quartiles. The dotted line extends to 1.5 times the interquartile distance.

by their median values. The latter show an evident correspondence between eIF6 and aIF6 at their natural conditions, thus confirming the *corresponding states* found by MSDs, EISFs, etc. (above).

Dynamic Effects of the Loose C-Terminal Tail. In the first section, we have shown that the presence of an additional his-tag tail to aIF6 makes the scattering functions and MSD from aIF6-htag similar to those of eIF6. To further investigate this equivalence, we performed MD simulations of aIF6-htag (aIF6 with the his-tag) and eIF6 without the Ctail (eIF6-not in the following) at ambient and high-temperature/high-pressure conditions. Figure 12 presents variations of RMSF between structurally corresponding residues in different IF6s with and without the additional tail. The RMSFs of C_α in aIF6 and eIF6-not are very similar to each other both at ambient and extreme conditions, with their differences being rarely larger than 0.5 Å. The same effect holds for eIF6 and aIF6-htag. This observation is also confirmed by the average all-atom RMSFs shown in Table 4. Moreover, the observed differences are of the same order of magnitude as those found in the RMSF of aIF6 and eIF6 when compared with their respective "natural" conditions. These results suggest that the Ctail in eIF6 is essential to achieving structural flexibility similar to that of aIF6 at high temperature and pressure, again in accordance with the corresponding states hypothesis. While His-tag and Ctail are bound to opposite termini of the conserved structure (N- and C-terminal, respectively), the impact on flexibility is comparable because of their spatial proximity (their C_α are 6 Å distant from each other). These two tails do not appear to have direct interactions with the rest of the protein structure; they are far enough away to make the mediation of hydration water rather improbable, and their insertion in protein sequences does not significantly alter the amino acid percentage compositions (Table 1).

A disordered character of protein tails is widely found in proteins. Similarly to the picture proposed here for IF6, tails which do not interact with other structured parts of the protein are found to utilize their high flexibility and entropic nature for protein function. By moving around their points of attachment, these extended protrusions may, for instance, sweep out significant portions of space and entropically exclude large particles, allowing instead small molecules such as water, salts, or cofactors to approach.[64] Alternatively, they may contribute to modulate the timing for the formation of protein−protein complexes.[65] It is also worth noting that intrinsically disordered terminal domains are usually susceptible to proteolysis and prone to post translational modifications,[66] as has been reported for Ctail.[30] A disordered C-terminal tail was also found to play a crucial role for specific proteins in assisting the biogenesis of diverse noncoding RNA precursors.[67] On the whole, these observations give a few examples of the plethora of functionalities related to terminal tails.[68] They also suggest that, although the presence of Ctail seems not to be necessary for the eIF6 antiassociation function,[30] it may have an active role in helping eIF6 to perform one of its other functions[31] for which an appropriate flexibility (the same as aIF6 at extreme conditions) is required.

DISCUSSION AND CONCLUSION

We have shown, for the first time to our knowledge, that pressure has a role in determining the dynamic properties of thermo-barophilic proteins, in this case from *M. jannaschii*. The extremophilic (aIF6) and mesophilic (eIF6) homologues

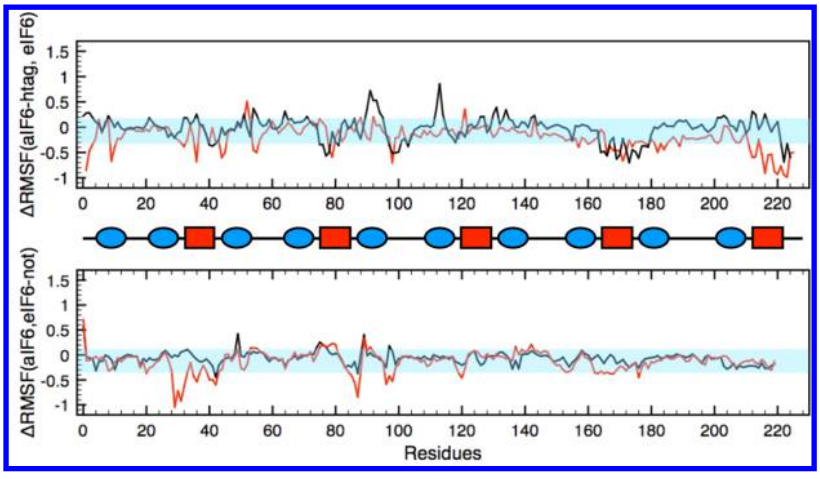

Figure 12. Analysis of the RMSF of the carbon C_α position from aIF6-htag and eIF6-not backbone. Upper panel: Differences of RMSF from aIF6-htag and eIF6 at similar conditions. Lower panel: Differences of RMSF from aIF6 and eIF6-not at similar conditions. Black lines refer to RMSFs obtained from simulations at 300 K and 1 bar, while red ones, to 350 K and 500 bar. Cyan horizontal bands represent the standard deviation of RMSF values between aIF6 at 350 K and 750 bar and eIF6 at 300 K and 1 bar.

DOI: 10.1021/acs.jpcb.5b02034
J. Phys. Chem. B 2015, 119, 7860−7873

show similar overall flexibility at their respective natural conditions, revealing the existence of "corresponding states" previously proposed for thermophilic proteins.

State-of-the-art QENS experiments have been performed to investigate the $P-T$ dependence of IF6 dynamics, but the signal-to-noise ratio of the data is still limited due to the use of dilute protein solutions and pressure cells. The data has been fitted with scattering functions obtained from MD simulations for the proteins used in the measurements (with a His-tag for aIF6) on the corresponding time scale and temperature/pressure conditions. These independent but complementary QENS and MD techniques give consistent information on the IF6 dynamics. The validated MD models have then been used to thoroughly investigate different aspects of the "corresponding states".

MSDs show that increasing the temperature to 350 K brings the overall molecular flexibility of aIF6 up and close to that of eIF6 at room temperature, with pressure causing smaller changes in flexibility. Incoherent scattering functions, that are observed experimentally, reveal the same changes in flexibility but also include spatial information through the Q-dependence of the signal. Differences in flexibility between proteins as a function of temperature and pressure occur in the 15−40 nm^{-1} range, which corresponds to 1.5−4 Å in real space. On the time scale of the experiments and the MD simulations, flexibility is modified on the local scale of amino acids and their side chains. Analysis of the scattering functions using the fOU model shows that aIF6 and eIF6 have different relaxation times but their internal motion is characterized by similar "effective potentials", suggesting a mainly entropic contribution to the similar flexibilities found in aIF6 and eIF6. The latter is reflected in the α-parameter, which determines the form of the relaxation rate spectrum (eq 4) and thus the heterogeneity of the relaxation processes.

Pressure is used to fine-tune molecular flexibility and therefore the "corresponding states". Structure dependent analysis of the EISF shows that backbone flexibility of aIF6 is suppressed with increasing pressure, but this is compensated by increased mobility of the amino acid side chains. The deep-sea pressure of 750 bar appears to be an optimal pressure, above which less significant changes occur. Structural flexibility has also been investigated directly via the residue-dependent RMSF and backbone straightness. Flexibility of aIF6 changes most significantly with pressure and temperature in the bending regions between helices and beta-strands.

The most striking structural difference between the IF6 proteins is the Ctail on eIF6. Large amplitude diffusion of this 20 amino acid tail confers the necessary structural flexibility on eIF6 under ambient conditions, that is matched by aIF6 at high temperature and pressure. Cleaving the Ctail from eIF6 produces dynamics similar to that of aIF6, while adding a His-tag to aIF6, as was required for the experimental work and the corresponding simulations, produces dynamics similar to that of eIF6. Incidentally, this finding also suggests that, although the existing practice of adding polyhistidine tags or removing disordered tails to facilitate protein structure determination seems to be reliable,[69] this may not be the case when studying dynamic properties or enzyme activity.[58]

MATERIALS AND METHODS

Experimental Setup. *Sample Preparation.* All samples were prepared as also described in other studies.[30] A full description of the expression and purification protocols is given as Supporting Information. The estimation of the concentration of final protein solutions was made by UV−vis spectroscopy and gave a value of ∼40 mg/ml. The measurements of the hydrodynamic radius of eIF6 were performed with a DynaPro-Titan fixed-angle light scattering system.

Neutron Scattering Experiments and Analysis. The QENS experiments at ambient pressure presented in this article were performed on the time-of-flight spectrometer FOCUS at the Paul Scherrer Institut in Zurich. The neutron spectra were measured with an incident neutron wavelength of λ = 6 Å corresponding to an elastic q-range of 0.3−2.3 $Å^{-1}$. The elastic energy resolution determined by vanadium standard runs was ΔE = 0.040 meV (half width at half-maximum). Experiments have been performed at different temperatures on protein deuterated solutions and on the corresponding buffer. Buffer runs are used to evaluate the solvent contribution in the solution runs in order to isolate the contribution arising from the protein alone.

The QENS spectra at high pressure were recorded on the time-of-flight spectrometer IN6 at the Institut Laue-Langevin in Grenoble. The pressure cell was developed at the Institut Laue Langevin in Grenoble (France) and was conceived to carry out experiments on liquid solutions at moderate high pressure. In particular, the dimensions of the cylindrical geometry were determined to withstand pressure up to 2 kbar: internal diameter of 10 mm and wall thickness of 1.5 mm. The global geometry of the cell was inspired by the one previously used for high pressure studies on lysozyme.[47] In contrast to the latter, however, here the pressure is applied without transmitting media and directly on the sample which is compressed by a pump connected to the pressure cell by a very thin capillary (0.1 mm diameter). Moreover, the irradiated part of the cell was made of an alloy of copper-berylium which permitted the wall thickness to be significantly reduced without affecting their mechanical resistance. In order to reduce the multiple scattering due to the protein solution, an insert with a diameter of 9 mm was used. As a whole, the pressure system required a total volume of ∼3 mL of protein solution which is considerably smaller than the volume commonly used in this type of QENS experiments and suitable for the typical amount of aIF6 /eIF6 production yields. The strong scattering by the pressure cell was corrected for.

All QENS data at ambient and high pressure were corrected for detector efficiency, normalized to the integrated vanadium intensity, converted to the energy scale, as well as converted from constant scattering angle θ to constant momentum transfer q.

Molecular Modeling. *Molecular Dynamics Simulations.* Molecular dynamics simulations of aIF6 and eIF6, together with the two *toy* structures, eIF6-not and aIF6-htag, were performed using the AMBER9 simulation package.[70] The whole set of simulations followed the same general protocol: coordinates of the missing hydrogen atoms were added using the algorithms implemented in the LEaP program from the AMBER9 package; the protein was placed in a orthorhombic periodic box filled with around 8000 water molecules parametrized by the TIP3P model; the whole system, including also sodium (Na+) counterions, was initially minimized and then equilibrated by a short simulation of 150 ps in a NVT ensemble, i.e., with fixed total volume and temperature kept equal to 300 K, followed by a 700 ps long simulation in the final NPT ensemble, with T = 300 K and P = 1 bar; in each simulation, the control of temperature was performed with a

DOI: 10.1021/acs.jpcb.5b02034
J. Phys. Chem. B 2015, 119, 7860−7873

Langevin thermostat with a collision rate of 3.5 ps^{-1}, whereas pressure was constrained by a Berendsen barostat relaxation time of τ_p = 1.5 ps; atomic interactions were modeled by the AMBER99SB all-atom force field.[71] The length of the production runs at each temperature−pressure value is reported in Table 3. More details on the molecular modeling protocols used in this work are given as Supporting Information. Global motions (translation and rotation) were removed beforehand from all trajectories in order to avoid the presence of unwanted spurious contributions in the calculation of correlation functions of interest.[72,73] The computation of neutron scattering spectra from MD simulations was performed using the package nMoldyn.[74]

Analysis. *Neutron Scattering Data.* In neutron scattering experiments, the measured quantity is the number of neutrons scattered by the sample into a specific solid angle element and a limited range of energy. The incoherent part of this quantity is proportional to the dynamic structure factor

$$S(q, \omega) = \frac{1}{2\pi}\int_{-\infty}^{+\infty} \mathrm{d}t\, \exp(-i\omega t) I(q, t) \tag{5}$$

where $I(q, t)$ is the incoherent intermediate scattering function (ISF), which depends on the positions of the dominantly scattering hydrogen atoms

$$I(q, t) = \frac{1}{N_H}\sum_{k\in \mathbb{H}} \langle \exp(iq[x_k(t) - x_k(0)])\rangle \tag{6}$$

Here N_H is the number of hydrogen atoms in the sample and $q = |\mathbf{q}|$ is the modulus of the momentum transfer which the neutron transfers to the sample. In addition, the following assumptions are made:

- The hydrogen content in the proteins under consideration corresponds to the natural abundance, i.e., about 50%, such that incoherent scattering from hydrogen dominates by far all other scattering processes.
- The momentum transfer $\hbar q$ is moderate and quantum effects in the sample can be neglected, as far as QENS is concerned.
- The sample is isotropic, and the coordinate "x" stands for a displacement in an arbitrary direction.

The long time limit of $I(q,t)$, which exists only for spatially confined motions, is the elastic incoherent structure factor (EISF)

$$\mathrm{EISF}(q) = \lim_{t\to\infty} I(q, t) \tag{7}$$

which can be approximated as

$$\mathrm{EISF}(q) \approx \frac{1}{N_H}\sum_{k\in \mathbb{H}} \exp(-q^2\langle x_k{}^2\rangle) \tag{8}$$

assuming that all atoms move in an isotropic harmonic potential and that the heterogeneity of the motional amplitudes for different atoms can be neglected.[75] As discussed elsewhere,[47] one may define $\langle x^2\rangle$ via

$$\langle x^2\rangle := -\frac{\ln(\mathrm{EISF}[q])}{q^2} \tag{9}$$

which leads to a *q-dependent* position fluctuation.

Analysis of Data from MD Simulations. The MD data used for this study describe internal protein dynamics, and to be useful for the direct comparison with QENS spectra of protein solutions, the effects of global diffusion and of finite instrumental resolution must be incorporated.

Neglecting multiple scattering effects and absorption, and assuming that global diffusion of the IF6 molecules and internal motions are decoupled, we write the overall dynamic structure factor as a convolution product (defining $(f * g)(\omega) = \int_{-\infty}^{+\infty} \mathrm{d}\omega' f(\omega - \omega')g(\omega')$):

$$S_m(q, t) = (S_{int} * S_g * r)(\omega) \tag{10}$$

Here S_{int} stands for the dynamic structure factor accounting for internal motions (calculated from the MD simulations), S_g is a Lorentzian describing global translational diffusion (D_a is the diffusion constant)

$$S_g(\omega) = \frac{1}{\pi}\frac{D_a q^2}{(D_a q^2)^2 + \omega^2} \tag{11}$$

and r is the resolution function. The latter is well described by a Gaussian, $r(\omega) = (2\pi)^{1/2}/\sigma \exp(-\omega^2/(2\sigma)^2)$, with $\sigma > 0$ and a half width at half-maximum (HWHM) of $\Delta E \approx 1.17\sigma$. $S_g(.)$ is normalized such that $\int_{-\infty}^{+\infty} \mathrm{d}\omega S_g(\omega) = 1$. The shape of $r(\omega)$ was fitted onto the experimental spectra from vanadium. We note that global rotational diffusion can be neglected here, since it is too small to be detectable by the spectrometers used in this study.

Diffusion Coefficient for a Torus. The derivation of the translational diffusion coefficient for a body of toroidal shape can be found in ref 76. Assuming rotational and translational diffusion as decoupled, one obtains for the translational part

$$D_{torus} = \frac{K_B T}{8\pi\mu a}\left(\log\left(\frac{8a}{b}\right) + \frac{1}{2}\right) \tag{12}$$

where a and b are the *inner* and *outer* radius, respectively, and μ is the solvent viscosity. For IF6s, the values of a and b are calculated averaging over the distance of α-carbons in the residues flanking the central hollow, for a, and in the five opposite sides of the pentameric pseudosymmetry, for b. The values of μ used in our analysis are $\mu_{300K} = 1.11 \times 10^{-3}$ Pa·s and $\mu_{350K} = 0.45 \times 10^{-3}$ Pa·s for heavy water at 300 and 350 K, respectively.

Backbone Straightness. Kinks and pivoting points in backbone structure as well as their variations upon different thermodynamic conditions were detected by the analysis of the mean square fluctuations of the "straightness" parameter σ, defined according to the ScrewFit algorithm.[77,78] The latter allows for the characterization of protein structures by combining quaternionic representation of rotation matrices and Chasles' theorem on rigid-body displacements. When applied to subsequent peptide planes in protein structures, ScrewFit gives local helical parameters of the protein backbone winding. For each pair of consecutive peptide planes, ScrewFit defines three parameters indicating their relative orientation and distance from a common axis of rotation (the axis of screw motion). The straightness parameter is then the scalar product between the unit vectors of local axes of screw motion, relative to four consecutive peptide planes. It gives information about local curvatures of a protein backbone tract. Large values of $\langle\Delta\sigma^2\rangle$ over a set of protein conformations indicate pivoting regions where the backbone constantly kinks.

Side-Chain Order Parameter. The order parameter Θ_{χ_α} for the side-chain dihedral angle χ_α was calculated, according to ref 79, as

DOI: 10.1021/acs.jpcb.5b02034
J. Phys. Chem. B 2015, 119, 7860−7873

$$\Theta_{\chi} = \frac{1}{N}\left|\sum_{i=1}^{N}\overrightarrow{\chi_{\alpha,i}}\right| \quad (13)$$

where N is the number of structures in the MD trajectories and $\overrightarrow{\chi_i}$ is a two-dimensional unit vector whose phase is equal to the dihedral angle χ_α in structure i. Values close to unity indicate very narrow dihedral angle distributions and therefore bonds that are rigid with respect to rotation. Values close to zero indicate dihedral angles defined over uniform distribution. In the present work, to equally consider the contribution of each side chain, without taking into account its length, we limited our analysis only to the order parameter for side-chain dihedral angle χ_1.

■ ASSOCIATED CONTENT

Supporting Information

Experimental procedures for sample production together with a detailed description of the molecular modeling of aIF6, eIF6, eIF6-not, and aIF6-htag. The Supporting Information is available free of charge on the ACS Publications website at DOI: 10.1021/acs.jpcb.5b02034.

■ AUTHOR INFORMATION

Corresponding Authors

*E-mail: paolo.calligari@unipd.it.
*E-mail: johnson@ill.eu.
*E-mail: gerald.kneller@cnrs-orleans.fr.

Present Address

[▽]Chemistry Department, University of Padua, Italy.

Notes

The authors declare no competing financial interest.

■ ACKNOWLEDGMENTS

P.A.C. acknowledges the International School for Advanced Studies (NOFYSAS 2012 Grants For Young Researchers) for funding.

■ REFERENCES

(1) Morell, V. Life's last domain. *Science* **1996**, *273*, 1043−1045.
(2) Somero, G. Adaptations to high hydrostatic pressure. *Annu. Rev. Physiol.* **1992**, *54*, 557−577.
(3) Rothschild, L.; Mancinelli, R. Life in extreme environments. *Nature* **2001**, *409*, 1092−1102.
(4) Tsou, C. Folding of the nascent peptide chain into a biologically active protein. *Biochemistry* **1988**, *27*, 1809−1812.
(5) Jaenicke, R. Protein stability and molecular adaptation to extreme conditions. *Eur. J. Biochem.* **1991**, *202*, 715−728.
(6) Zaccai, G. How soft is a protein? A protein dynamics force constant measured by neutron scattering. *Science* **2000**, *288*, 1604−1607.
(7) Jaenicke, R. Stability and stabilization of globular proteins in solution. *J. Biotechnol.* **2000**, *79*, 193−203.
(8) Vihinen, M. Relationship of protein flexibility to thermostability. *Protein Eng.* **1987**, *1*, 477.
(9) Závodszky, P.; Kardos, J.; Svingor, A.; Petsko, G. A. Adjustment of conformational flexibility is a key event in the thermal adaptation of proteins. *Proc. Natl. Acad. Sci. U.S.A.* **1998**, *95*, 7406−7411.
(10) Tehei, M.; Madern, D.; Franzetti, B.; Zaccai, G. Neutron Scattering Reveals the Dynamic Basis of Protein Adaptation to Extreme Temperature. *J. Biol. Chem.* **2005**, *280*, 40974−40979.
(11) Tehei, M.; Zaccai, G. Adaptation to high temperatures through macromolecular dynamics by neutron scattering. *FEBS J.* **2007**, *274*, 4034−4043.
(12) Grottesi, A.; Ceruso, M.; Colosimo, A.; Nola, A. D. Molecular dynamics study of a hyperthermophilic and a mesophilic rubredoxin. *Proteins* **2002**, *46*, 287−294.
(13) Hernández, G.; Jenney, F.; Adams, M.; LeMaster, D. Millisecond time scale conformational flexibility in a hyperthermophile protein at ambient temperature. *Proc. Natl. Acad. Sci. U.S.A.* **2000**, *97*, 3166.
(14) Razvi, A.; Scholtz, J. Lessons in stability from thermophilic proteins. *Protein Sci.* **2006**, *15*, 1569.
(15) Orecchini, A.; Paciaroni, A.; Francesco, A. D.; Petrillo, C.; Sacchetti, F. Collective dynamics of protein hydration water by brillouin neutron spectroscopy. *J. Am. Chem. Soc.* **2009**, *131*, 4664−4669.
(16) Stadler, A. M.; Embs, J. P.; Digel, I.; Artmann, G. M.; Unruh, T.; Büldt, G.; Zaccai, G. Cytoplasmic water and hydration layer dynamics in human red blood cells. *J. Am. Chem. Soc.* **2008**, *130*, 16852−16853.
(17) Schiró, G.; Caronna, C.; Natali, F.; Cupane, A. Direct evidence of the amino acid side chain and backbone contributions to protein anharmonicity. *J. Am. Chem. Soc.* **2010**, *132*, 1371−1376.
(18) Tehei, M.; Madern, D.; Pfister, C.; Zaccai, G. Fast dynamics of halophilic malate dehydrogenase and BSA measured by neutron scattering under various solvent conditions influencing protein stability. *Proc. Natl. Acad. Sci. U.S.A.* **2001**, *98*, 14356−14361.
(19) Kurkal-Siebert, V.; Smith, J. C. Low-temperature protein dynamics: a simulation analysis of interprotein vibrations and the boson peak at 150K. *J. Am. Chem. Soc.* **2006**, *128*, 2356−2364.
(20) Busch, S.; Smuda, C.; Pardo, L. C.; Unruh, T. Molecular mechanism of long-range diffusion in phospholipid membranes studied by quasielastic neutron scattering. *J. Am. Chem. Soc.* **2010**, *132*, 3232−3233.
(21) Mikl, C.; Peters, J.; Trapp, M.; Kornmueller, K.; Schneider, W. J.; Prassl, R. Softness of atherogenic lipoproteins: a comparison of very low density lipoprotein (VLDL) and low density lipoprotein (LDL) using elastic incoherent neutron scattering (EINS). *J. Am. Chem. Soc.* **2011**, *133*, 13213−13215.
(22) Miao, Y.; Yi, Z.; Glass, D. C.; Hong, L.; Tyagi, M.; Baudry, J.; Jain, N.; Smith, J. C. Temperature-dependent dynamical transitions of different classes of amino acid residue in a globular protein. *J. Am. Chem. Soc.* **2012**, *134*, 19576−19579.
(23) Hay, S.; Evans, R. M.; Levy, C.; Loveridge, E. J.; Wang, X.; Leys, D.; Allemann, R. K.; Scrutton, N. S. Are the catalytic properties of enzymes from piezophilic organisms pressure adapted? *ChemBioChem* **2009**, *10*, 2348−2353.
(24) Li, W.; Hoffman, D. Structure and dynamics of translation initiation factor aIF-1A from the archaeon Methanococcus jannaschii determined by NMR spectroscopy. *Protein Sci.* **2001**, *10*, 2426−2438.
(25) Tehei, M.; Franzetti, B.; Madern, D.; Ginzburg, M.; Ginzburg, B. Z.; Giudici-Orticoni, M.-T.; Bruschi, M.; Zaccai, G. Adaptation to extreme environments: macromolecular dynamics in bacteria compared in vivo by neutron scattering. *EMBO Rep.* **2004**, *5*, 66−70.
(26) Wang, H.; Boisvert, D.; Kim, K. K.; Kim, R.; Kim, S. H. Crystal structure of a fibrillarin homologue from Methanococcus jannaschii, a hyperthermophile, at 1.6 A resolution. *EMBO J.* **2000**, *19*, 317−323.
(27) Michels, P.; Clark, D. Pressure enhanced activity and stability of a hyperthermophilic protease from a deep-sea methanogen. *Appl. Environ. Microbiol.* **1997**, *63*, 3985−3991.
(28) Miller, J.; Shah, N.; Nelson, C.; Ludlow, J.; Clark, D. Pressure and Temperature Effects on Growth and Methane Production of the Extreme Thermophile Methanococcus jannaschii. *Appl. Environ. Microbiol.* **1988**, *54*, 3039−3042.
(29) Hawley, S. Reversible Pressure-Temperature Denaturation of Chymotrypsinogen. *Biochemistry* **1971**, *10*, 2436−2442.
(30) Groft, C. M.; Beckmann, R.; Sali, A.; Burley, S. K. Crystal structures of ribosome anti-association factor IF6. *Nat. Struct. Biol.* **2000**, *7*, 1156−1164.
(31) Miluzio, A.; Beugnet, A.; Volta, V.; Biffo, S. Eukaryotic initiation factor 6 mediates a continuum between 60S ribosome biogenesis and translation. *EMBO Rep.* **2009**, *10*, 459−465.

DOI: 10.1021/acs.jpcb.5b02034
J. Phys. Chem. B 2015, 119, 7860−7873

(32) Benelli, D.; Marzi, S.; Mancone, C.; Alonzi, T.; Teana, A. L.; Londei, P. Function and ribosomal localization of aIF6, a translational regulator shared by archaea and eukarya. *Nucleic Acids Res.* **2009**, *37*, 256−267.
(33) Basu, U.; Si, K.; Deng, H.; Maitra, U. Phosphorylation of Mammalian Eukaryotic Translation Initiation Factor 6 and Its Saccharomyces cerevisiae Homologue Tif6p: Evidence that Phosphorylation of Tif6p Regulates Its Nucleocytoplasmic Distribution and Is Required for Yeast Cell Growth. *Mol. Cell. Biol.* **2003**, *23*, 6187−6199.
(34) Sanvito, F.; Piatti, S.; Villa, A.; Bossi, M.; Lucchini, G.; Marchisio, P.; Biffo, S. The β4 integrin interactor p27(BBP/eIF6) is an essential nuclear matrix protein involved in 60S ribosomal subunit assembly. *J. Cell Biol.* **1999**, *144*, 823−837.
(35) Senger, B.; Lafontaine, D. L.; Graindorge, J.-S.; Gadal, O.; Camasses, A.; Sanni, A.; Garnier, J.-M.; Breitenbach, M.; Hurt, E.; Fasiolo, F. The Nucle(ol)ar Tif6p and Efl1p Are Required for a Late Cytoplasmic Step of Ribosome Synthesis. *Mol. Cell* **2001**, *8*, 1−20.
(36) Ceci, M.; Gaviraghi, C.; Gorrini, C.; Sala, L. A.; Offenhauser, N.; Marchisio, P.; Biffo, S. Release of eIF6 (p27BBP) from the 60S subunit allows 80S ribosome assembly. *Nature* **2003**, *426*, 579−584.
(37) Kneller, G. Quasielastic neutron scattering and relaxation processes in proteins: Analytical and simulation-based models. *Phys. Chem. Chem. Phys.* **2005**, *7*, 2641−2655.
(38) Shao, Y. The fractional Ornstein-Uhlenbeck process as a representation of homogeneous Eulerian velocity turbulence. *Phys. D (Amsterdam, Neth.)* **1995**, *83*, 461−477.
(39) Metzler, R.; Klafter, J. The random walk's guide to anomalous diffusion: a fractional dynamics approach. *Phys. Rep.* **2000**, *339*, 1−77.
(40) Uhlenbeck, G.; Ornstein, L. On the theory of the Brownian motion. *Phys. Rev.* **1930**, *36*, 823.
(41) Glöckle, W.; Nonnenmacher, T. A fractional calculus approach to self-similar protein dynamics. *Biophys. J.* **1995**, *68*, 46−53.
(42) Yang, H.; Xie, X. Probing single-molecule dynamics photon by photon. *J. Chem. Phys.* **2002**, *117*, 10965−10979.
(43) Yang, H.; Luo, G.; Karnchanaphanurach, P.; Louie, T.; Rech, I.; Cova, S.; Xun, L.; Xie, X. Protein conformational dynamics probed by single-molecule electron transfer. *Science* **2003**, *302*, 262−266.
(44) Kneller, G.; Hinsen, K. Fractional Brownian dynamics in proteins. *J. Chem. Phys.* **2004**, *121*, 10278−10283.
(45) Calandrini, V.; Kneller, G. Influence of pressure on the slow and fast fractional relaxation dynamics in lysozyme: A simulation study. *J. Chem. Phys.* **2008**, *128*, No. 065102.
(46) Calandrini, V.; Abergel, D.; Kneller, G. Protein dynamics from a NMR perspective: Networks of coupled rotators and fractional Brownian dynamics. *J. Chem. Phys.* **2008**, *128*, 145102.
(47) Calandrini, V.; Hamon, V.; Hinsen, K.; Calligari, P.; Bellissent-Funel, M.-C.; Kneller, G. R. Relaxation dynamics of lysozyme in solution under pressure: Combining molecular dynamics simulations and quasielastic neutron scattering. *Chem. Phys.* **2008**, *345*, 289−297.
(48) Calligari, P.; Calandrini, V.; Kneller, G. R.; Abergel, D. From NMR relaxation to fractional brownian dynamics in proteins: results from a virtual experiment. *J. Phys. Chem. B* **2011**, *115*, 12370−12379.
(49) Calligari, P.; Abergel, D. Toward the Characterization of Fractional Stochastic Processes Underlying Methyl Dynamics in Proteins. *J. Phys. Chem. B* **2012**, *116*, 12955−12965.
(50) Calligari, P.; Abergel, D. Multiple scale dynamics in proteins probed at multiple time scales through fluctuations of NMR chemical shifts. *J. Phys. Chem. B* **2014**, *118*, 3823−3831.
(51) Haney, P. J.; Badger, J. H.; Buldak, G. L.; Reich, C. I.; Woese, C. R.; Olsen, G. J. Thermal adaptation analyzed by comparison of protein sequences from mesophilic and extremely thermophilic Methanococcus species. *Proc. Natl. Acad. Sci. U.S.A.* **1999**, *96*, 3578−3583.
(52) Vieille, C.; Zeikus, G. Hyperthermophilic enzymes: sources, uses, and molecular mechanisms for thermostability. *Microbiol. Mol. Biol. Rev.* **2001**, *65*, 1−43.
(53) Balbo, A.; Bozzaro, S. Cloning of Dictyostelium eIF6 (p27BBP) and mapping its nucle(ol)ar localization subdomains. *Eur. J. Cell Biol.* **2006**, *85*, 1069−1078.
(54) Jones, D. Protein secondary structure prediction based on position-specific scoring matrices. *J. Mol. Biol.* **1999**, *292*, 195−202.
(55) Raghava, G. APSSP2: A combination method for protein secondary structure prediction based on neural network and example based learning. *CASP5* **2002**, *A*, 132.
(56) Kyte, J.; Doolittle, R. A simple method for displaying the hydropathic character of a protien. *J. Mol. Biol.* **1982**, *157*, 105.
(57) Valenzuela, D. M.; Chaudhuri, A.; Maitra, U. Eukaryotic ribosomal subunit anti-association activity of calf liver is contained in a single polypeptide chain protein of Mr = 25,500 (eukaryotic initiation factor 6). *J. Biol. Chem.* **1982**, *257*, 7712−7719.
(58) Freydank, A.; Brandt, W.; Dräger, B. Protein structure modeling indicates hexahistidine-tag interference with enzyme activity. *Proteins* **2008**, *72*, 173−183.
(59) Erdélyi, A.; Magnus, W.; Oberhettinger, F.; Tricomi, F. *Higher Transcendental Functions*; McGraw Hill: New York, 1953.
(60) Bée, M. *Quasielastic Neutron Scattering: Principles and Applications in Solid State Chemistry Biology and Materials Science*; Adam Hilger: Bristol, 1988.
(61) Kneller, G.; Calandrini, V. Estimating the influence of finite instrumental resolution on elastic neutron scattering intensities from proteins. *J. Chem. Phys.* **2007**, *126*, 125107.
(62) Kalimeri, M.; Rahaman, O.; Melchionna, S.; Sterpone, F. How conformational flexibility stabilizes the hyperthermophilic elongation factor G-domain. *J. Phys. Chem. B* **2013**, *117*, 13775−13785.
(63) Merkley, E.; Parson, W.; Daggett, V. Temperature dependence of the flexibility of thermophilic and mesophilic flavoenzymes of the nitroreductase fold. *Protein Eng., Des. Sel.* **2010**, *23*, 327.
(64) Hoh, J. H. Functional protein domains from the thermally driven motion of polypeptide chains: a proposal. *Proteins* **1998**, *32*, 223−228.
(65) Magidovich, E.; Orr, I.; Fass, D.; Abdu, U.; Yifrach, O. Intrinsic disorder in the C-terminal domain of the Shaker voltage-activated K+ channel modulates its interaction with scaffold proteins. *Proc. Natl. Acad. Sci. U.S.A.* **2007**, *104*, 13022−13027.
(66) Sudnitsyna, M. V.; Mymrikov, E. V.; Seit-Nebi, A. S.; Gusev, N. B. The role of intrinsically disordered regions in the structure and functioning of small heat shock proteins. *Curr. Protein Pept. Sci.* **2012**, *13*, 76−85.
(67) Kucera, N. J.; Hodsdon, M. E.; Wolin, S. L. An intrinsically disordered C terminus allows the La protein to assist the biogenesis of diverse noncoding RNA precursors. *Proc. Natl. Acad. Sci. U.S.A.* **2011**, *108*, 1308−1313.
(68) Uversky, V. N. The most important thing is the tail: multitudinous functionalities of intrinsically disordered protein termini. *FEBS Lett.* **2013**, *587*, 1891−1901.
(69) Carson, M.; Johnson, D.; McDonald, H.; Brouillette, C. His-tag impact on structure. *Acta Crystallogr., Sect. D* **2007**, *63*, 295−301.
(70) Case, D.; Darden, T.; Cheatham, T., III; Simmerling, C.; Wang, J.; Duke, R.; Luo, R.; Merz, K.; Pearlman, D.; Crowley, M.; et al. *AMBER 9*; University of California: San Francisco, CA, 2006.
(71) Hornak, V.; Abel, R.; Okur, A.; Strockbine, B.; Roitberg, A.; Simmerling, C. Comparison of multiple Amber force fields and development of improved protein backbone parameters. *Proteins* **2006**, *65*, 712−725.
(72) Kneller, G. Superposition of Molecular Structures using Quaternions. *Mol. Simul.* **1991**, *7*, 113−119.
(73) Chevrot, G.; Calligari, P.; Hinsen, K.; Kneller, G. R. Least constraint approach to the extraction of internal motions from molecular dynamics trajectories of flexible macromolecules. *J. Chem. Phys.* **2011**, *135*, 084110.
(74) Rog, T.; Murzyn, K.; Hinsen, K.; Kneller, G. nMoldyn: A Program Package for a Neutron Scattering Oriented Analysis of Molecular Dynamics Simulations. *J. Comput. Chem.* **2003**, *24*, 657−667.
(75) Kneller, G. R.; Chevrot, G. Impact of anisotropic atomic motions in proteins on powder-averaged incoherent neutron scattering intensities. *J. Chem. Phys.* **2012**, *137*, 225101.

DOI: 10.1021/acs.jpcb.5b02034
J. Phys. Chem. B 2015, 119, 7860−7873

(76) Thaorak, R. Brownian motion of a torus. *Colloids Surf., A* **2008**, *317*, 650−657.
(77) Kneller, G. R.; Calligari, P. Efficient characterization of protein secondary structure in terms of screw motions. *Acta Crystallogr., Sect. D* **2006**, *62*, 302−311.
(78) Calligari, P. A.; Kneller, G. R. ScrewFit: combining localization and description of protein secondary structure. *Acta Crystallogr., Sect. D* **2012**, *68*, 1690−1693.
(79) Hyberts, S. G.; Goldberg, M. S.; Havel, T. F.; Wagner, G. The solution structure of eglin c based on measurements of many NOEs and coupling constants and its comparison with X-ray structures. *Protein Sci.* **1992**, *1*, 736−751.

DOI: 10.1021/acs.jpcb.5b02034
J. Phys. Chem. B 2015, 119, 7860−7873